

AN ANALYTIC MODEL OF THE PHYSICAL PROPERTIES OF GALAXY CLUSTERS

G. ESRA BULBUL¹, NICOLE HASLER¹, MASSIMILIANO BONAMANTE^{1,2} AND MARSHALL JOY²

Draft version May 27, 2022

ABSTRACT

We introduce an analytic model of the diffuse intergalactic medium in galaxy clusters based on a polytropic equation of state for the gas in hydrostatic equilibrium with the cluster gravitational potential. This model is directly applicable to the analysis of X-ray and Sunyaev-Zeldovich Effect observations from the cluster core to the virial radius, with 5 global parameters and 3 parameters describing the cluster core. We validate the model using *Chandra* X-ray observations of two polytropic clusters, MS 1137.5+6625 and CL J1226.9+3332, and two cool core clusters, Abell 1835 and Abell 2204. We show that the model accurately describes the spatially resolved spectroscopic and imaging data, including the cluster core region where significant cooling of the plasma is observed.

Subject headings: X-rays: galaxies: clusters-galaxies: individual (MS 1137.5+6625, CL J1226.9+3332, Abell 1835, Abell 2204)

1. INTRODUCTION

Galaxy cluster masses play an important role in addressing fundamental physical and cosmological problems, such as the measurement of the cluster gas mass fraction (Allen et al. 2008; Ettori et al. 2009), the evolution of the growth of structure (Mantz et al. 2008, 2009; Vikhlinin et al. 2009), and the gravitational sedimentation of ions (Chuzhoy & Nusser 2003; Peng & Nagai 2009; Shtykovskiy & Gilfanov 2010). A vital tool for the measurement of cluster masses is the diffuse hot intergalactic medium which can be detected primarily through its bright X-ray emission (Sarazin 1988), or through the Sunyaev-Zeldovich Effect (SZE, Sunyaev & Zel'dovich 1972; Carlstrom et al. 2002). A variety of models are used to describe the distribution of the gas, from the simple isothermal β model (Cavaliere & Fusco-Femiano 1976; Birkinshaw et al. 1991) to more complex models that describe either the X-ray properties (gas density and temperature, Vikhlinin et al. 2006; Cavaliere et al. 2009) or the SZE properties (gas pressure, Nagai et al. 2007; Mroczkowski et al. 2009; Arnaud et al. 2009).

We investigate a model of galaxy clusters based on an analytic distribution for the cluster mass density inspired by the Navarro et al. (1996) distribution, which we generalize following Suto et al. (1998), Ascasibar et al. (2003) and Ascasibar & Diego (2008) to include a variable asymptotic slope at large radii. This mass density is combined with a polytropic equation of state for the gas, to provide self-consistent density, temperature and pressure profiles for a plasma in hydrostatic equilibrium. The use of a polytropic equation of state for the cluster gas has also been recently proposed by Ascasibar & Diego (2008) and Bode et al. (2009), and tested observationally by Sanderson & Ponman (2009).

In this paper we derive analytic radial profiles for the physical quantities (temperature, density and pressure) relevant to X-ray and SZE observations, and

present an application of these models to high resolution *Chandra* observations of the galaxy clusters MS 1137.5+6625, CL J1226.9+3332, Abell 1835 and Abell 2204. Applications of this new model include measurement of gas mass fraction from joint X-ray and Sunyaev-Zeldovich Effect observations (Hasler et al. 2010) and the effect of He sedimentation on X-ray mass estimates (Bulbul et al. 2010). This paper is organized as follows: in §2 we describe our model, in §3 we present the application of the model to *Chandra* X-ray observations of MS 1137.5+6625, CL J1226.9+3332, Abell 2204 and Abell 1835, and in §4 we perform a comparison between our mass measurements and the results of Mroczkowski et al. (2009). In §5 we present our conclusions. In the analysis of the *Chandra* data we assume the cosmological parameters $h = 0.73$, $\Omega_M = 0.27$ and $\Omega_\Lambda = 0.73$.

2. A MODEL OF THE INTERGALACTIC MEDIUM BASED ON HYDROSTATIC EQUILIBRIUM AND THE POLYTROPIC EQUATION OF STATE

2.1. The Mass Density Distribution

The cluster gravitational potential is dominated by dark matter, with the intergalactic medium and stars contributing less than approximately $\sim 20\%$ of the mass (Allen et al. 2004, 2008; Ettori et al. 2009; Vikhlinin et al. 2009). We therefore start with a total mass density distribution that is obtained as a generalization of the Navarro et al. (1996) profile:

$$\rho_{tot}(r) = \frac{\rho_i}{(r/r_s)(1+r/r_s)^\beta} \quad (1)$$

where ρ_i is the normalization constant, r_s is a characteristic scale radius and $\beta+1$ is the slope of the density distribution at large radii. Equation 1 is a simplified version of the density distribution introduced by Suto et al. (1998).

The total mass enclosed within radius r can be found by taking the volume integral of the density (Equation 1):

$$M(r) = \frac{4\pi\rho_i r_s^3}{(\beta-2)} \left(\frac{1}{\beta-1} + \frac{1/(1-\beta) - r/r_s}{(1+r/r_s)^{\beta-1}} \right). \quad (2)$$

¹ Department of Physics, University of Alabama, Huntsville, AL 35899

² Space Science Office, VP62, NASA Marshall Space Flight Center, Huntsville, AL 35812

Equation 2 is indeterminate at $\beta = 2$; the limit at $\beta = 2$ can be determined using L'Hospital's rule:

$$M(r) = 4\pi\rho_i r_s^3 \left(\ln(1 + r/r_s) - \frac{r/r_s}{1 + r/r_s} \right) \quad [\beta = 2] \quad (3)$$

and therefore the mass is a continuous function of β with no discontinuity at $\beta = 2$.

The gravitational potential at a distance r is found by

$$d\phi(r) = GM(r)/r^2 dr \quad (4)$$

using the boundary condition $\phi(\infty) = 0$. Equation 4 can be integrated analytically

$$\phi(r) = \phi_0 \left(\frac{1}{(\beta - 2)} \frac{(1 + r/r_s)^{\beta-2} - 1}{r/r_s(1 + r/r_s)^{\beta-2}} \right), \quad (5)$$

where

$$\phi_0 = -\frac{4\pi G\rho_i r_s^2}{(\beta - 1)}. \quad (6)$$

The potential at $\beta = 2$ is also found by using L'Hospital's rule,

$$\phi(r) = \phi_0 \left(\frac{\ln(1 + r/r_s)}{r/r_s} \right) \quad [\beta = 2]. \quad (7)$$

Therefore the gravitational potential is a continuous function of β with no discontinuity at $\beta = 2$. Figure 1 shows the radial distribution of the gravitational potential for $1.0 \leq \beta \leq 3.0$. The limiting value of $\beta = 1$ is

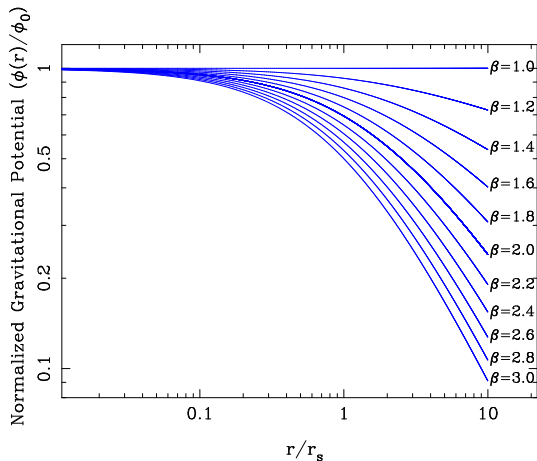


FIG. 1.— Normalized gravitational potential for various values of the β parameter.

shown in Figure 1, corresponding to a constant potential.

2.2. Gas Density and Temperature Profile

The diffuse gas is assumed to be in hydrostatic equilibrium with the gravitational potential. Assuming spherical symmetry,

$$\frac{1}{\mu m_p n_e(r)} \frac{dP_e}{dr} = -\frac{d\phi(r)}{dr} \quad (8)$$

where $P_e(r) = n_e(r)kT(r)$ is the electron pressure, G denotes the gravitational constant, m_p is the proton mass, μ is the mean molecular weight of the plasma, k is

the Boltzmann constant and $n_e(r)$ is the electron number density. In order to solve Equation 8, we assume that the gas follows a polytropic equation of state,

$$\frac{n_{e,poly}(r)}{n_{e0}} = \left[\frac{T_{poly}(r)}{T_0} \right]^n \quad (9)$$

where n is the polytropic index, n_{e0} and T_0 are the values of the number density and temperature at $r = 0$. The polytropic index $n > 0$ is a free parameter of the model, with the limit $n \rightarrow \infty$ describing an isothermal distribution of gas (Eddington 1926).

The temperature profile is obtained as a function of the gravitational potential from Equations 8 and 9,

$$T_{poly}(r) = -\frac{1}{(n+1)} \frac{\mu m_p}{k} \phi(r) \quad (10)$$

and therefore, using Equation 5,

$$T_{poly}(r) = T_0 \left(\frac{1}{(\beta - 2)} \frac{(1 + r/r_s)^{\beta-2} - 1}{r/r_s(1 + r/r_s)^{\beta-2}} \right), \quad (11)$$

where the normalization constant T_0 is obtained from Equations 6 and 10:

$$T_0 = \frac{4\pi G\mu m_p}{k(n+1)} \frac{r_s^2 \rho_i}{(\beta - 1)}. \quad (12)$$

Equation 10 shows that $T_{poly}(r) \propto \phi(r)$, and therefore Figure 1 also describes $T_{poly}(r)$ as function of radius. Equation 12 links the gas temperature to the normalization of the matter density ρ_i , and therefore the depth of the gravitational potential can be determined from the observed temperature profile.

Using the relation between temperature and gas density provided by the polytropic relation (Equation 9), the polytropic gas density profile is

$$n_{e,poly}(r) = n_{e0} \left(\frac{1}{(\beta - 2)} \frac{(1 + r/r_s)^{\beta-2} - 1}{r/r_s(1 + r/r_s)^{\beta-2}} \right)^n. \quad (13)$$

2.3. The Electron Gas Pressure

The gas pressure is obtained using the ideal gas law $P_e(r) = n_{e,poly}kT_{poly}(r)$,

$$P_e(r) = P_{e0} \left(\frac{1}{(\beta - 2)} \frac{(1 + r/r_s)^{\beta-2} - 1}{r/r_s(1 + r/r_s)^{\beta-2}} \right)^{n+1} \quad (14)$$

In the limit $\beta \rightarrow 2$ the pressure is analytically described by

$$P_e(r) = P_{e0} \left(\frac{\ln(1 + r/r_s)}{r/r_s} \right)^{n+1} \quad [\beta = 2]. \quad (15)$$

The electron pressure for this model has only 4 free parameters, and it is suitable for the analysis of Sunyaev-Zeldovich Effect observations of galaxy clusters (Hasler et al. 2010).

2.4. Cool Core Clusters

Although the temperature profile predicted by the polytropic model provides a good description at intermediate to large radii, cool core clusters feature a significant temperature drop in the central region which cannot be approximated by a polytropic equation of state (see for example, Vikhlinin et al. 2005; Sanderson et al. 2006; Vikhlinin et al. 2006; Baldi et al. 2007). For cool core clusters we introduce a modified temperature profile

$$T(r) = T_{poly}(r)\tau_{cool}(r) \quad (16)$$

where $T_{poly}(r)$ is the temperature profile according to the polytropic equation of state (Equation 11) and $\tau_{cool}(r)$ is a phenomenological core taper function used by Vikhlinin et al. (2006):

$$\tau_{cool}(r) = \frac{\alpha + (r/r_{cool})^\gamma}{1 + (r/r_{cool})^\gamma}, \quad (17)$$

where $0 < \alpha < 1$ is a free parameter that measures the amount of central cooling and r_{cool} is a characteristic cooling radius. The temperature profile modified by the core taper function is shown in Figure 2 for representative values of parameters r_{cool} , γ and α .

Therefore, the explicit temperature profile for cool core clusters is given by

$$T(r) = T_0 \left(\frac{1}{(\beta - 2)} \frac{(1 + r/r_s)^{\beta-2} - 1}{r/r_s(1 + r/r_s)^{\beta-2}} \right) \tau_{cool}(r). \quad (18)$$

In order to calculate the density distribution for cool core clusters, we assume that the pressure distribution is the same as in the polytropic case (Equation 14). Therefore, the electron density is given by

$$\begin{aligned} n_e(r) &= \frac{P_e(r)}{kT(r)} \\ &= n_{e0} \left(\frac{1}{(\beta - 2)} \frac{(1 + r/r_s)^{\beta-2} - 1}{r/r_s(1 + r/r_s)^{\beta-2}} \right)^n \tau_{cool}^{-1}(r) \end{aligned} \quad (19)$$

The behavior of the gas density for various core taper parameters is shown in Figure 2.

For hydrostatic equilibrium to be satisfied, these modified density and temperature distributions require a modified total mass distribution:

$$M(r) = \frac{4\pi\rho_i r_s^3}{(\beta - 2)} \left(\frac{1}{\beta - 1} + \frac{1/(1 - \beta) - r/r_s}{(1 + r/r_s)^{\beta-1}} \right) \tau_{cool}(r). \quad (20)$$

The only difference between the cool core total mass distribution (Equation 20) and the polytropic total mass distribution (Equation 2) is the term $\tau_{cool}(r)$, which is significant only at small radii. At large radii, the effect of the core taper vanishes, and the thermodynamics of the gas is described by the polytropic equation of state.

3. APPLICATION TO *Chandra* OBSERVATIONS OF CLUSTERS

3.1. *Chandra* Data Reduction and Analysis

We use deep *Chandra* ACIS-I observations of four galaxy clusters to validate our models: two clusters which

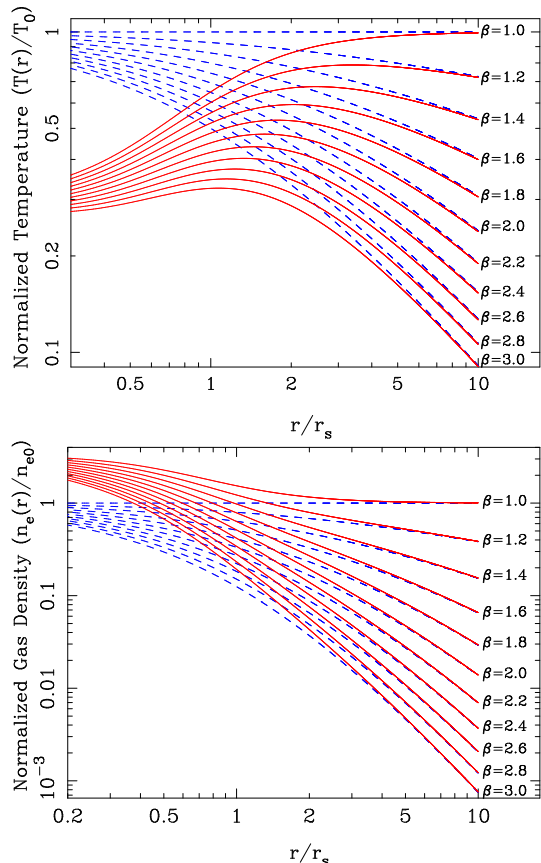


FIG. 2.— Solid red lines are the normalized temperature and density profiles for a taper function with parameters $\alpha = 0.3$, $r_{cool} = r_s$ and $\gamma = 2.0$, and variable values for β ; blue dashed lines are the models without the core taper function.

do not have a cool core component, MS 1137.5+6625 and CL J1226.9+3332, and two cool core clusters, Abell 2204 and Abell 1835. The observations are summarized in Table 1. As part of the data reduction procedure, we applied afterglow, bad pixel and charge transfer inefficiency corrections to the Level 1 event files using CIAO 4.1 and CALDB 4.1.1. Flares in the background due to solar activity are eliminated using light curve filtering as described in Markevitch et al. (2003). Filtered exposure times are also given in Table 1.

For the purpose of background subtraction we use blank-sky observations. Given that the background is obtained from regions of the sky that may have different soft X-ray fluxes than at the cluster position, we use a peripheral region of the ACIS-I detector to model the difference between the blank-sky and the cluster soft fluxes. This step in the analysis is particularly important for Abell 2204, which lies in a region of significantly higher soft X-ray emission than the average blank-sky region. Spectra and images used in this paper are extracted in the energy band 0.7-7.0 keV, chosen to minimize the effect of calibration uncertainties at the lowest energies, and the effect of the detector background at high energy.

Spectra are extracted in concentric annuli surrounding the centroid of X-ray emission after all point sources were removed. An optically thin plasma emission model (APEC in XSPEC) is used, with temperature, abundance and normalization as free parameters. The redshift and Galactic N_H of the four clusters are shown in Table 1.

TABLE 1
CLUSTER SAMPLE

| Cluster | z | N_H^a (cm^{-2}) | Obs. ID | Exposure Time (ksec) |
|-----------------|--------------------|---------------------------------|--------------|-------------------------|
| Abell 2204 | 0.152 ^b | 5.67×10^{20} | 7940 | 72.9 |
| Abell 1835 | 0.252 ^b | 2.04×10^{20} | 6880 | 110.0 |
| MS 1137.5+6625 | 0.784 ^c | 9.54×10^{19} | 536 | 115.5 |
| CL J1226.9+3332 | 0.888 ^d | 1.38×10^{20} | 5014 3180 | 32.7 31.5 |

(a) Leiden/Argentine/Bonn (LAB) Survey, see Kalberla et al. (2005)

(b) Struble & Rood (1999)

(c) Donahue et al. (1999)

(d) Ebeling et al. (2001)

TABLE 2
SOURCES OF SYSTEMATIC ERROR IN THE *Chandra* DATA

| Source of uncertainty | Observable affected | Fractional Error |
|-----------------------------------|-------------------------|------------------|
| Background level | Background count rate | 5% |
| Spatial variations of A_{eff}^a | Photon count rates | 1% |
| Energy calibration of A_{eff}^b | Temperature measurement | 5% |

(a) Reference: <http://cxc.harvard.edu/cal/>

(b) Reference: http://cxc.harvard.edu/ciao4.1/why/caldb4.1.1_hrma.html

3.2. Systematic Uncertainties in the *Chandra* Data Analysis

We consider possible sources of systematic uncertainty in the *Chandra* data. The blank-sky background used in our analysis is normalized to the high-energy background level of each cluster observation, determined from peripheral regions of the ACIS detector that are free of cluster emission (following Markevitch et al. 2003). The primary source of uncertainty in the background subtraction is the choice of a peripheral region as representative of the background at the cluster location. Due to the scatter in the count rate of various peripheral regions in each cluster observation, we estimate a $\sim 5\%$ uncertainty in the determination of the background level from these *Chandra* observations. We use this uncertainty in the spectral and imaging data analysis.

Calibration of the ACIS effective area is another significant source of systematic uncertainty in our analysis. For the spectral data used for measuring the gas temperature, the primary source of uncertainty is the low-energy calibration of the effective area and the presence of a contaminant on the optical filter of the ACIS detector. We use the *Chandra* calibration available in CALDB 4.1.1, which includes a significant change in the effective area calibration which improves the agreement between clusters temperatures obtained with ACIS-I, and also with other instruments (such as *XMM-Newton*'s EPIC). With this calibration of the *Chandra* efficiency we estimate that any residual systematic error in the measurement of cluster temperatures is of order $\sim 5\%$, and add this error to the temperature measured in each bin.

For the imaging data, spatially-dependent non-uniformities in the ACIS efficiency are a relevant source of possible systematic error because of the extended nature of the sources. The absolute calibration of the ACIS efficiency is currently at the level of 3%, with possible spatial variations on arcmin scales at the level of $\sim 1\%$;

we use a 1% error as additional uncertainty in the count rates for each annulus.

Table 2 provides a summary of the uncertainties included in our analysis of the *Chandra* data, and references to the *Chandra* calibration information.

3.3. Result of Model Fits and Mass Measurements

The radial profiles of the X-ray surface brightness and temperature observed from the *Chandra* data are used to determine the best-fit parameters and the goodness of fit for MS 1137.5+6625, CL J1226.9+3332, Abell 1835 and Abell 2204. The X-ray surface brightness is

$$S_x = \frac{1}{4\pi(1+z)^3} \int n_e^2 \Lambda_{ee}(T) dl, \quad (21)$$

where S_x is in detector units (counts cm^{-2} arcmin $^{-2}$ s $^{-1}$), z is the cluster redshift, $\Lambda_{ee}(T)$ is the plasma emissivity in detector units (counts cm^3 s $^{-1}$) which we calculate using the APEC code (Smith et al. 2001) and l is the distance along the line of sight.

We validate the model using two polytropic clusters which do not have a cool core component, MS 1137.5+6625 and CL J1226.9+3332, and two cool core clusters Abell 1835 and Abell 2204. We use the Monte Carlo Markov Chain code described in Bonamente et al. (2004) for the fit. The model described in § 2 has 8 free parameters, of which 5 parameters describe the global cluster properties (n_{e0} , T_{e0} , r_s , β , n) and 3 additional parameters (r_{cool} , α , γ) are used to model the central region of the cool core clusters.

3.3.1. Polytropic Clusters MS 1137.5+6625 and CL J1226.9+3332

For polytropic clusters, which do not have a cool core component, 5 parameters are sufficient to describe the distribution of density, temperature. We fixed β to 2 for

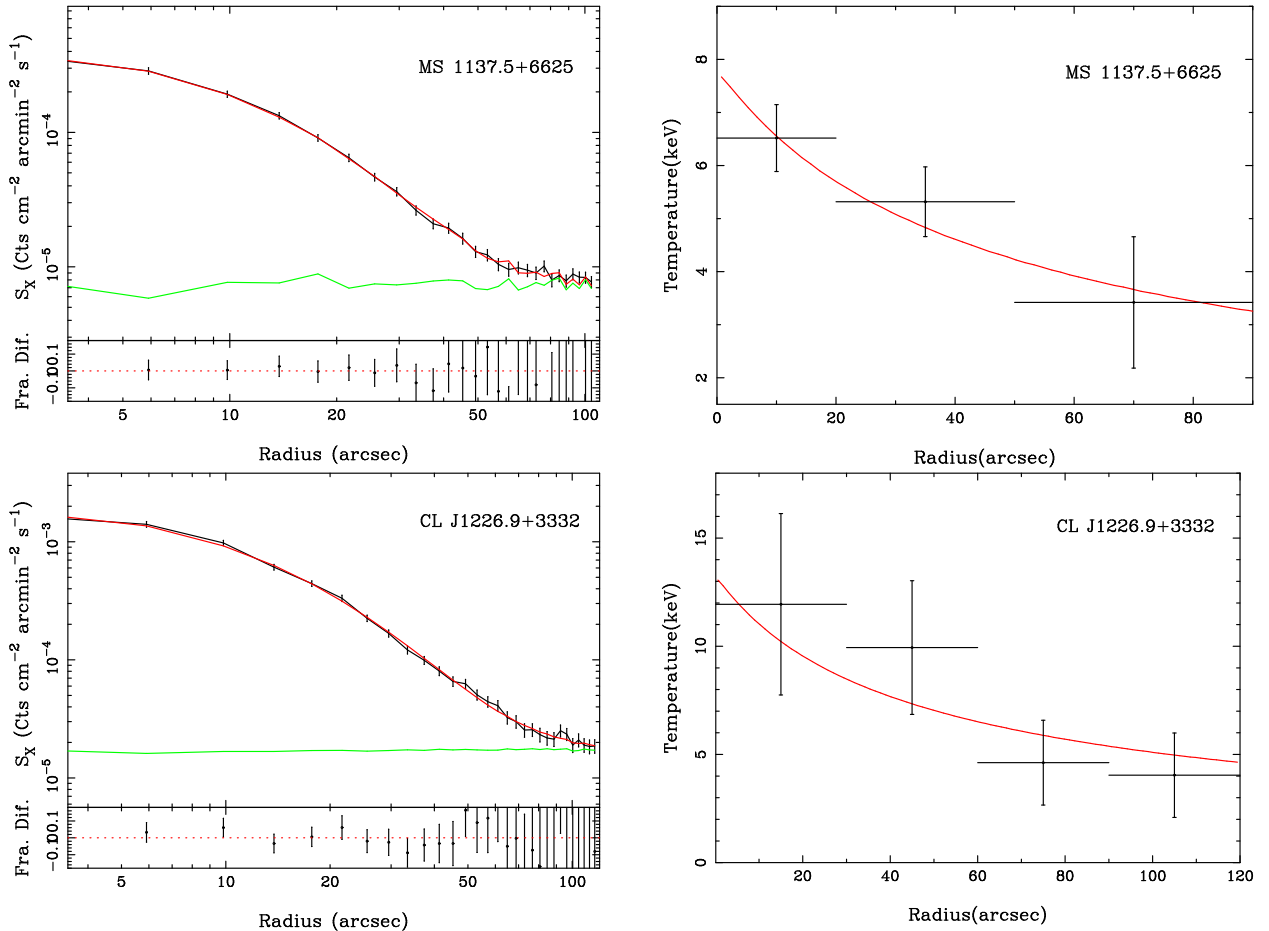


FIG. 3.— X-ray surface brightness and temperature profiles of MS 1137.5+6625 in the radial range 0 - 90 '' and CL J1226.9+3332 in the radial range 0 - 120 ''. The red line in both profiles shows the best fit model to the data; the green line in surface brightness profiles shows the background level. The overall χ^2 of the fit (Table 3) is the sum of the χ^2 values of the surface brightness profile and the temperature profile.

TABLE 3
BEST-FIT PARAMETERS OF THE MODEL

| Cluster | n_{e0} (10^{-2} cm^{-3}) | r_s (arcsec) | n | β | T_0 (keV) | r_{cool} (arcsec) | α | γ | χ^2 (d.o.f.) | P value |
|-----------------|---|--------------------------|------------------------|------------------------|-------------------------|-------------------------|------------------------|----------|-------------------|-----------|
| MS 1137.5+6625 | $2.17^{+0.07}_{-0.19}$ | $23.84^{+10.88}_{-2.19}$ | $4.83^{+1.30}_{-0.27}$ | 2.0 | $7.84^{+1.08}_{-1.26}$ | - | - | - | 14.4 (26) | 96.7 % |
| CL J1226.9+3332 | $3.99^{+0.23}_{-0.23}$ | $22.65^{+5.06}_{-2.79}$ | $4.54^{+0.54}_{-0.31}$ | 2.0 | $13.32^{+2.28}_{-2.98}$ | - | - | - | 14.6 (29) | 98.8% |
| Abell 2204 | $4.42^{+0.37}_{-0.24}$ | $21.73^{+1.50}_{-2.01}$ | $6.44^{+1.02}_{-0.51}$ | $1.39^{+0.04}_{-0.06}$ | $14.28^{+0.75}_{-0.78}$ | $19.42^{+0.60}_{-0.73}$ | $0.16^{+0.01}_{-0.01}$ | 2.0 | 115.5 (145) | 96.6% |
| Abell 1835 | $2.57^{+0.29}_{-0.07}$ | $40.32^{+3.29}_{-6.48}$ | $3.98^{+0.73}_{-0.41}$ | $1.94^{+0.15}_{-0.22}$ | $18.26^{+0.42}_{-1.61}$ | $22.65^{+0.28}_{-1.17}$ | $0.18^{+0.02}_{-0.01}$ | 2.0 | 99.3 (93) | 30.8% |

these clusters (Navarro et al. 1996), since the polytropic index (n) and β cannot both be determined from X-ray data available. We report the χ^2 of the best-fit model for MS 1137.5+6625 and CL J1226.9+3332 in Table 3. We also calculate the gas mass by taking the volume integral of Equation 13 and the total mass using Equation 2 and report the results in Table 4.

3.3.2. Cool Core Clusters Abell 2204 and Abell 1835

The clusters Abell 2204 and Abell 1835 have a clear cool core component (see Figure 4), which requires the use of the cooling equations described in §2.4. The best fit model parameters are listed in Table 3. We also calcu-

late the gas mass by taking the volume integral of Equation 19 and the total mass using Equation 20 and report the results in Table 4.

4. COMPARISON WITH PREVIOUS WORK

In Table 5 we present the comparison of mass measurements of Abell 1835 produced from the polytropic model with the masses reported in Mroczkowski et al. (2009) at r_{2500} and r_{500} . For this purpose we calculate gas mass and total mass at the same radii r_{2500} and r_{500} as in Mroczkowski et al. (2009), and use the same Gaussian uncertainty on r_{Δ} in order to have a fair comparison on masses. The gas mass measurements pro-

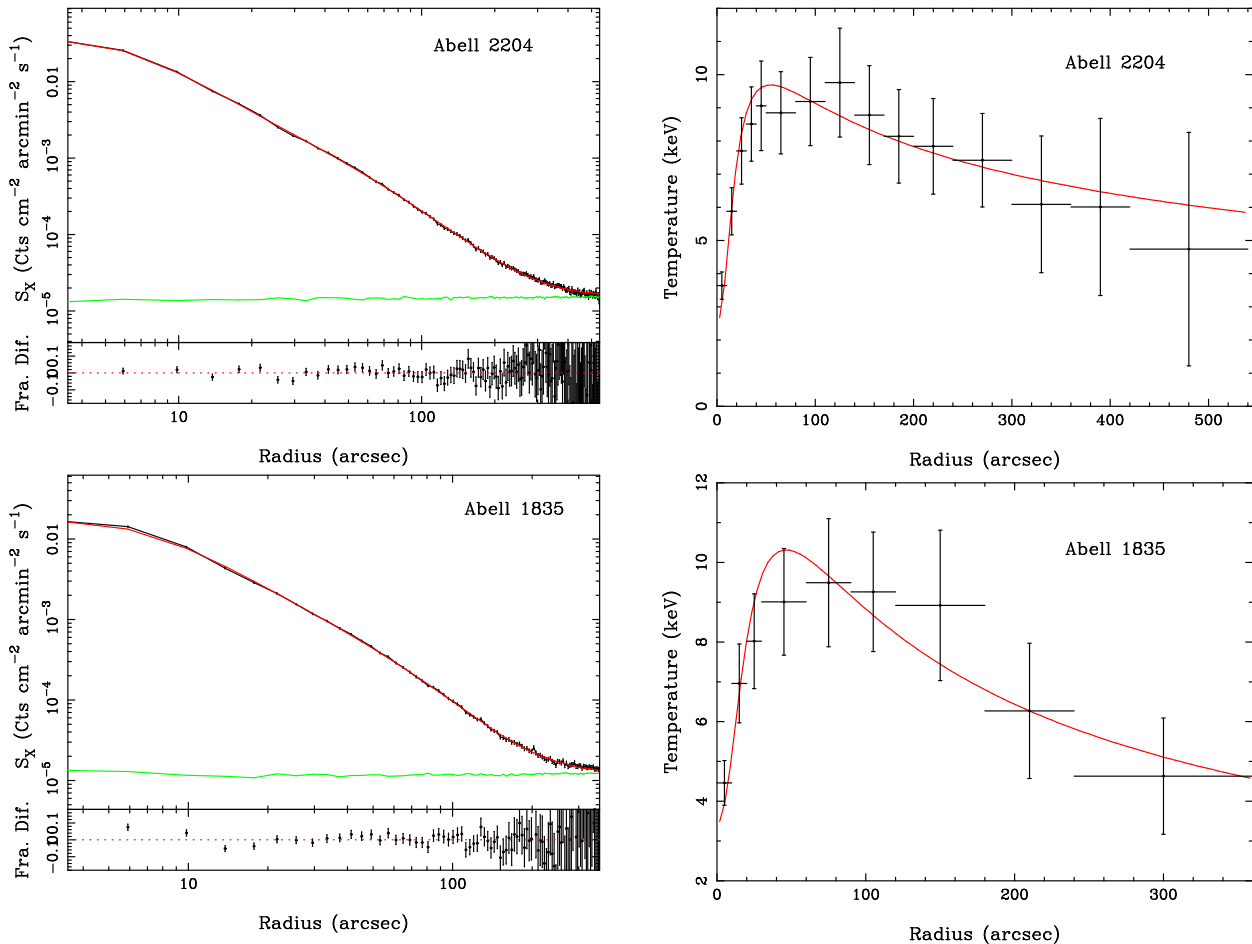


FIG. 4.— X-ray surface brightness and temperature profiles of cool core clusters Abell 2204 in the radial range 0 - 540 '' and Abell 1835 in the radial range 0 - 360 ''. The red line in both profiles shows the best fit model to the data; the green line shows the background level. The overall χ^2 of the fit (Table 3) is the sum of the χ^2 values of the surface brightness profile and the temperature profile.

TABLE 4
GAS AND TOTAL MASSES

| Cluster | r_{2500} (arcsec) | $M_{gas}(r_{2500})$ ($10^{13} M_{\odot}$) | $M_{tot}(r_{2500})$ ($10^{14} M_{\odot}$) | r_{500} (arcsec) | $M_{gas}(r_{500})$ ($10^{13} M_{\odot}$) | $M_{tot}(r_{500})$ ($10^{14} M_{\odot}$) |
|-----------------|------------------------|--|--|-------------------------|---|---|
| MS 1137.5+6625 | $44.7^{+4.1}_{-3.8}$ | $1.10^{+0.13}_{-0.11}$ | $1.20^{+0.36}_{-0.28}$ | $98.5^{+9.6}_{-8.2}$ | $3.08^{+0.13}_{-0.13}$ | $2.56^{+0.82}_{-0.59}$ |
| CL J1226.9+3332 | $48.8^{+4.7}_{-5.3}$ | $3.01^{+0.39}_{-0.44}$ | $2.16^{+0.69}_{-0.63}$ | $104.6^{+9.1}_{-10.4}$ | $8.29^{+0.55}_{-0.63}$ | $4.25^{+1.22}_{-1.14}$ |
| Abell 2204 | $225.7^{+4.1}_{-4.1}$ | $3.99^{+0.09}_{-0.09}$ | $3.37^{+0.19}_{-0.18}$ | $479.8^{+11.4}_{-11.2}$ | $10.35^{+0.26}_{-0.26}$ | $6.47^{+0.47}_{-0.44}$ |
| Abell 1835 | $150.6^{+3.4}_{-4.2}$ | $4.97^{+0.14}_{-0.17}$ | $3.72^{+0.26}_{-0.30}$ | $309.7^{+9.8}_{-13.1}$ | $12.08^{+0.38}_{-0.50}$ | $6.47^{+0.64}_{-0.79}$ |

duced by the polytropic model are consistent with the Mroczkowski et al. (2009) results at the 1σ level (see Table 5).

The Chandra Calibration Database (CALDB) has recently been revised to correct the effective area, resulting in lower X-ray temperatures, especially for massive clusters¹. The peak X-ray temperatures reported by Mroczkowski et al. (2009) using CALDB 3.4 are ~ 2 keV greater than the temperatures derived in this paper using

the recent calibration (CALDB 4.1.1). From Equations 2 and 20, we estimate that this temperature change would reduce the total masses reported by Mroczkowski et al. (2009) by 17 % (see Table 5). When the X-ray temperature calibration issue is accounted for, the total mass values in Table 5 are in agreement within the stated 1σ uncertainties.

5. DISCUSSION AND CONCLUSIONS

We introduce a new model to describe the physical properties of the hot intra-cluster medium and present an application of the model to *Chandra* X-ray observations

¹ http://cxc.harvard.edu/caldb/downloads/Release_notes/CALDB_v4.1.1.html

TABLE 5
MASS COMPARISON OF ABELL 1835 WITH MROCKOWSKI ET AL. (2009)

| | r_{2500} arcsec | $M_{2500,gas}$ $10^{13} M_{sun}$ | $M_{2500,tot}$ $10^{14} M_{sun}$ | r_{500} arcsec | $M_{500,gas}$ $10^{13} M_{sun}$ | $M_{500,tot}$ $10^{14} M_{sun}$ |
|------------------------------|-----------------------|-------------------------------------|-------------------------------------|-------------------------|------------------------------------|------------------------------------|
| Abell 1835 | | | | | | |
| Mroczkowski et al. (2009) | $169.0^{+5.5}_{-8.0}$ | $5.77^{+0.25}_{-0.35}$ | $5.30^{+0.53}_{-0.72}$ [Note(a)] | $363.0^{+17.0}_{-12.0}$ | $13.94^{+0.64}_{-0.52}$ | $10.68^{+1.54}_{-1.01}$ [Note(b)] |
| Polytropic Model (this work) | $169.0^{+7.0}_{-7.0}$ | $5.79^{+0.35}_{-0.46}$ | $4.13^{+0.31}_{-0.32}$ | $363.0^{+15.0}_{-15.0}$ | $14.31^{+0.71}_{-0.82}$ | $7.37^{+0.82}_{-0.83}$ |

(a) When X-ray temperature is recalibrated using CALDB 4.1.1, mean value of $M_{2500,tot}$ decreases to $\sim 4.40 \times 10^{14} M_{sun}$
(b) When X-ray temperature is recalibrated using CALDB 4.1.1, mean value of $M_{500,tot}$ decreases to $\sim 8.86 \times 10^{14} M_{sun}$

of MS 1137.5+6625, CL J1226.9+3332, Abell 1835 and Abell 2204. The model is based on a polytropic equation of state for the gas in hydrostatic equilibrium with the cluster gravitational potential. Using a function for the cluster total mass density that has the asymptotic slope as a free parameter, we obtain analytic expressions for the gas density, temperature and pressure. We also include a core taper function that accounts for the cooling of the gas in the cluster center.

This model has a number of features that make it suitable for the analysis of X-ray and SZE observations of galaxy clusters. The model is analytic, and has a limited number of parameters which describe the global properties of the cluster. For clusters which do not have a cool core, 5 parameters are sufficient to describe the distribution of density, temperature, pressure and total matter density. The gas density and temperature are linked by the polytropic equation of state, and the total matter density is related to the plasma properties by the hydrostatic equation. Therefore there is just one scale radius (r_s) that appears in the radial distribution of all thermodynamic quantities. The other parameters that describe the global physical properties of the cluster are the central density (n_{e0}) and temperature (T_0) of the gas, the polytropic index n , and the asymptotic slope of the total mass density ($\beta + 1$). For cool core clusters, three

additional parameters allow an accurate description of the cooling of the gas in the core, and the accompanying increase in the density (§ 2.4).

In addition to the analysis of spatially-resolved spectroscopic and imaging X-ray data (see §3), the model is applicable to SZE observations, which require a model for the plasma pressure. A number of models suitable for SZE observations are available in the literature, for example Nagai et al. (2007) and Mroczkowski et al. (2009). Our model has the advantage of the simultaneous applicability to both X-ray and SZE observations, and it is therefore suitable for a number of cosmological applications including the measurement of the Hubble constant (Bonamente et al. 2006), the measurement of scaling relations between X-ray and SZE observables (Bonamente et al. 2008), the measurement of cluster masses independent of cosmology from joint X-ray and SZE data (Hasler et al. 2010) and the measurement of the effect of He sedimentation on X-ray measured masses (Bulbul et al. 2010).

ACKNOWLEDGMENTS

The authors would like to thank the referee, J. Carlstrom, D. Marrone and T. Mroczkowski for their useful comments on the manuscript.

REFERENCES

- Allen, S. W., Schmidt, R. W., Ebeling, H., Fabian, A. C., & van Speybroeck, L. 2004, *MNRAS*, 353, 457
Allen, S. W., Rapetti, D. A., Schmidt, R. W., Ebeling, H., Morris, R. G., & Fabian, A. C. 2008, *MNRAS*, 383, 879
Arnaud, M., Pratt, G. W., Piffaretti, R., Boehringer, H., Croston, J. H., & Pointecouteau, E. 2009, arXiv:0910.1234
Ascasibar, Y., & Diego, J. M. 2008, *MNRAS*, 383, 369
Ascasibar, Y., Yepes, G., Müller, V., & Gottlöber, S. 2003, *MNRAS*, 346, 731
Baldi, A., Ettori, S., Mazzotta, P., Tozzi, P., & Borgani, S. 2007, *ApJ*, 666, 835
Birkinshaw, M., Hughes, J. P., & Arnaud, K. A. 1991, *ApJ*, 379, 466
Bode, P., Ostriker, J. P., & Vikhlinin, A. 2009, *ApJ*, 700, 989
Bonamente, M., Joy, M. K., Carlstrom, J. E., Reese, E. D., & LaRoque, S. J. 2004, *ApJ*, 614, 56
Bonamente, M., Joy, M. K., LaRoque, S. J., Carlstrom, J. E., Reese, E. D., & Dawson, K. S. 2006, *ApJ*, 647, 25
Bonamente, M., Joy, M., LaRoque, S. J., Carlstrom, J. E., Nagai, D., & Marrone, D. P. 2008, *ApJ*, 675, 106
Bulbul, G. E. et al. 2010, in prep.
Carlstrom, J. E., Holder, G. P., & Reese, E. D. 2002, *ARA&A*, 40, 643
Cavaliere, A., & Fusco-Femiano, R. 1976, *A&A*, 49, 137
Cavaliere, A., Lapi, A., & Fusco-Femiano, R. 2009, *ApJ*, 698, 580
Chuzhoy, L., & Nusser, A. 2003, *MNRAS*, 342, L5
Donahue, M., Voit, G. M., Scharf, C. A., Gioia, I. M., Mullis, C. R., Hughes, J. P., & Stocke, J. T. 1999, *ApJ*, 527, 525
Ebeling, H., Jones, L. R., Fairley, B. W., Perlman, E., Scharf, C., & Horner, D. 2001, *ApJ*, 548, L23
Eddington, A. S. 1926, *The Internal Constitution of the Stars*, ed. A. S. Eddington
Ettori, S., Morandi, A., Tozzi, P., Balestra, I., Borgani, S., Rosati, P., Lovisari, L., & Terenziani, F. 2009, *A&A*, 501, 61
Hasler, N. et al. 2010, in prep.
Kalberla, P. M. W., Burton, W. B., Hartmann, D., Arnal, E. M., Bajaja, E., Morras, R., Poulmlppel, W. G. L. 2005, *A&A*, 440, 775
Mantz, A., Allen, S. W., Ebeling, H., & Rapetti, D. 2008, *MNRAS*, 387, 1179
Mantz, A., Allen, S. W., Rapetti, D., & Ebeling, H. 2009, *ArXiv e-prints*
Markevitch, M. et al. 2003, *ApJ*, 583, 70
Maughan, B. J., Jones, C., Jones, L. R., & Van Speybroeck, L. 2007, *ApJ*, 659, 1125
Mroczkowski, T. et al. 2009, *ApJ*, 694, 1034
Nagai, D., Kravtsov, A. V., & Vikhlinin, A. 2007, *ApJ*, 668, 1
Navarro, J. F., Frenk, C. S., & White, S. D. M. 1996, *ApJ*, 462, 563
—. 1997, *ApJ*, 490, 493
Peng, F., & Nagai, D. 2009, *ApJ*, 693, 839
Sanderson, A. J. R., Ponman, T. J., & O'Sullivan, E. 2006, *MNRAS*, 372, 1496

- Sanderson, A. J. R., & Ponman, T. J. 2009, ArXiv e-prints
- Sarazin, C. L. 1988, X-ray emission from clusters of galaxies (Cambridge Astrophysics Series, Cambridge: Cambridge University Press, 1988)
- Shtykovskiy, P., & Gilfanov, M. 2010, MNRAS, 401, 1360
- Smith, R. K., Brickhouse, N. S., Liedahl, D. A., & Raymond, J. C. 2001, ApJ, 556, L91
- Struble, M. F., & Rood, H. J. 1999, ApJS, 125, 35
- Sunyaev, R. A., & Zel'dovich, Y. B. 1972, Comments Astrophys. Space Phys., 4, 173
- Suto, Y., Sasaki, S., & Makino, N. 1998, ApJ, 509, 544
- Vikhlinin, A., Markevitch, M., Murray, S. S., Jones, C., Forman, W., & Van Speybroeck, L. 2005, ApJ, 628, 655
- Vikhlinin, A., Kravtsov, A., Forman, W., Jones, C., Markevitch, M., Murray, S. S., & Van Speybroeck, L. 2006, ApJ, 640, 691
- Vikhlinin, A. et al. 2009, ApJ, 692, 1060